HHS Public Access

Author manuscript

Conf Proc IEEE Eng Med Biol Soc. Author manuscript; available in PMC 2020 July 01.

Published in final edited form as:

Conf Proc IEEE Eng Med Biol Soc. 2019 July ; 2019: 6798–6801. doi:10.1109/EMBC.2019.8857051.

Stitching Stretchable Radiofrequency Coils for MRI: A Conductive Thread and Athletic Fabric Approach

Jana M. Vincent [Member, IEEE],

Weldon School of Biomedical Engineering and Department of Basic Medical Sciences, Purdue University, West Lafayette, IN 47907 USA.

Joseph V. Rispoli [Member, IEEE]

Weldon School of Biomedical Engineering and School of Electrical and Computer Engineering, Purdue University.

Abstract

Objective: We propose a novel flexible and entirely stretchable radiofrequency coil for magnetic resonance imaging. This coil design aims at increasing patient comfort during joint imaging while maintaining or improving image quality.

Methods: Conductive silver-coated thread was stitched in a zigzag pattern onto stretchable athletic fabric to create a single-loop receive coil. The stitched coil was mounted in a draped and stretched fashion and compared to a coil fabricated on flexible printed circuit board. Match/tune circuits, detuning circuits, and baluns were incorporated into the final setup for bench measurements and imaging on a 3T MR scanner. A fast spin echo sequence was used to obtain images for comparison.

Results: The fabricated coil presents multi-directional stretchability and flexibility while maintaining conductivity and stitch integrity. Quality factor measurements and SNR calculations show that this stretchable coil design is comparable to a flexible, standard PCB coil. Detailed human wrist images were successfully obtained *in vivo* using the stretched, stitched coil.

Conclusion: The resulting MR images and SNR calculations support further experimentation into more complex coil geometries.

Significance: This coil is uniquely stretchable in all direction and allows for joint imaging at various degrees of flexion. Additionally, this coil offers the closest proximity of placement to the skin with materials that provide a similar level of comfort to that of athletic wear and compression sleeves. This stitched design could be incorporated into coils for a variety of anatomies.

I. Introduction

Magnetic resonance imaging (MRI) is a noninvasive modality with the ability to reveal contrast between a broad range of tissues and joint components including muscle, cartilage, bone, ligaments, and tendons [1]. Radiofrequency (RF) receive coils are used to detect the localized NMR signal that is subsequently processed into the MR image. Typically, to

phone: 765-496-6431; fax: 765-496-1459; jmvincent@purdue.edu.

Author Manuscript

Author Manuscript

Author Manuscript

enhance the signal-to-noise ratio (SNR), receive coil arrays are shaped to encompass a generalized form of the anatomy of interest. Fixed coil arrays are durable and designed for specific applications, e.g., brain imaging; however, multiple sizes are often desirable to facilitate a closer fit and maximize SNR [2].Researchers have identified flexible coils as a means to improve SNR, with recently-proposed flexible or bendable planar RF coil designs fabricating coil conductors using screen-printing technology [3], copper braid [4], [5], and custom coaxial cable [6], [7]. These designs are well-suited for wrapping coil elements around an elliptic cylinder, e.g., the torso or abdomen. However, unidirectionally flexible coils do not facilitate MRI of convex joints such as the shoulder, knee, and elbow.

Millions of patients suffering from joint injuries and degenerative joint diseases, such as arthritis, have difficulty fully extending their joints [1], [8]. With increased life expectancies, it is estimated that more than 78 million individuals in the United States will be diagnosed with arthritis by the year 2040 [8]. Commercial joint-imaging RF coils are rigid and require the subject to lie in a pronated or supine position with the joint fully extended. Notably, a stretchable knee and wrist coil has been developed utilizing copper braid solder wick on a bandage designed to be stretched as it is wrapped around an area [4], [5]. Copper braiding is bendable but does not stretch, making a universal fit difficult. There is a need for a flexible and stretchable coil that enables comfortable positioning, particularly during lengthy MRI scans ranging from 20–60 minutes [9]. In addition to improving patient comfort, RF coil placement nearer the skin could enhance image quality since the coil is closer to the signal source.

In this work, we introduce a flexible and omnidirectionally stretchable RF coil. By utilizing conductive thread on athletic fabric, as opposed to copper or inks, the RF coils are able to stretch and bend like an athletic sleeve or compression band. We present results of both bench measurements and MRI experiments. Single-loop stretchable coils are evaluated at draped and stretched coil positions and compared with a flexible copper-trace surface coil. Lastly, we discuss the feasibility of employing this fabrication technique for coil arrays.

II. Materials and Methods

A. Coil Design

Two 71-mm (~3-in) single-loop receive coils were stitched on 90% polyester, 10% spandex athletic fabric with Lyofil thread (silver-coated, p-phenylene benzobisoxazole (PBO), Syscom Advanced Materials Inc., Columbus, OH, USA) and standard polyester bobbin thread (Fig. 1). In order to facilitate stretching, the preset zigzag stitch on a Brother JX2517 sewing machine (Brother International Corporation, Bridgewater, NJ, USA) was used. The stretched-to-draped coil radius ratio is 42.5:35.5 mm. A comparison coil was etched on flexible, 1-oz, 0.18-mm thick, copper-clad FR-4 printed circuit board (PCB) in a 76-mm (3-in) circle design with a trace width of 2.8 mm (Fig. 1). This coil was mounted to a custom 3D-printed half-cylindrical shell, with an inner diameter of 73 mm and outer diameter of 79 mm, designed to fit over a 1-L, 73-mm diameter, phantom bottle with an adhesive hook and loop fastener.

All coils were segmented on opposite sides allowing for the attachment of a match/tune board and variable capacitor (BFC280832659, Vishay Intertechnology, Malvern, PA, USA). A 27-pF capacitor was added, in series, adjacent to the match/tune board. This board also functions as a current trap, utilizing a 5-mm diameter tunable, unshielded inductor (165–00A06L, Coilcraft Inc., Cary, IL, USA) and PIN diode (MA4P7470F-1072T, MACOM, Lowell, MA, USA). The circuit diagram and board are shown in Fig. 2. One quarterwavelength of coaxial cable, including a balun, connected the coil upstream via a BNC connector.

B. Coil Testing: Bench Measurements

A network analyzer (E5071C, Keysight Technologies, Santa Rosa, CA, USA) was utilized in the tuning of both the trap and coils. Prior to tuning the trap, an S_{11} measurement was employed to match and tune the coil to the Larmor frequency of hydrogen at 3T (128 MHz) by adjusting the tuning capacitor, C_3. This tuning capacitor was then removed to create an open circuit and an S_{21} measurement was taken using a small, single-loop probe lightly coupled to the inductor and a second sniffer probe placed above the diode [10]. A DC power supply (1685B, B&K Precision Corporation, Yorba Linda, CA, USA) was connected to a series 10-Ω resistor to drive the PIN diode circuit. 5 V was supplied to forward bias the diode and the trap was tuned to 128 MHz. Subsequently, the tuning capacitor was reattached and adjusted so that the coil was matched and tuned using an S_{11} measurements with a bias of −5 V. These measurement were repeated for all coils.

After the matching and tuning of the coils were completed the coil quality factor (Q-factor) was calculated using the following formula specific to S_{11}, curve response [11] Where f_0 is the resonant frequency (Hz) and $\Delta f_{-7\mathrm{dB}}$ is the change in frequency (Hz) measured at the −7 dB crossings to the left and right of f_0:

$$Q = \frac{f_0}{\Delta f_{-7\mathrm{dB}}}. \tag{1}$$

Q-factors were calculated in both unloaded and phantom-loaded states. The phantom was a 1-L bottle comprised of 16.7 g of NaCl and 538 grams of sugar dissolved in 700 mL of water, as determined using the NIH recipe generator [12] to simulate the dielectric properties of human muscle, which has a permittivity of 63.5 and a conductivity of 0.719 S/m as determined through the IT'IS Foundation Tissue Properties Database [13]. 0.7 g of $CuSO_4$ was added to shorten the longitudinal relaxation time (T_1). Muscle was chosen due to the future intent to use these coils for joint imaging. To consider the influence of variable proximity to the load for a rigid coil, the mounted PCB coil was positioned in two locations: wrapped tightly around the phantom and mounted 4.2 cm above the phantom. This 4.2 cm spacing was chosen because it reflected the average distance between the skin and surface of a rigid commercial array coil for one test case.

C. Coil Testing: MRI Experiments

Coil testing was performed on a whole-body 3T MR scanner (Discovery MR750, GE Healthcare, Chicago, IL, USA). Each coil was connected individually to a receiver gateway box (16xRx, Clinical MR Solutions, Brookfield, WI, USA) and positioned as previously described around the aforementioned muscle phantom (Fig. 3). A fast spin-echo (FSE) sequence was executed with the following parameters: echo time (T_E) 120 ms, slice thickness 10 mm, pixel size 0.7 mm × 0.7 mm, grid 256 × 256. The built-in body coil was used to transmit, while the stitched coils and PCB coil were receive-only. All cases were acquired during the same scanning session and included a localizer, calibration, and FSE.

After scanning, data were imported into MATLAB (Mathworks, Natick, MA, USA). Using in-house code, SNR was calculated following the alternate single-image SNR measurement procedure prescribed by NEMA [14]. A 7 × 7-pixel region of signal and 11 × 11-pixel regions of noise were selected. These regions of selection are illustrated in Fig. 4.The in-house code was validated by corresponding SNR calculations using OsiriX Lite (Pixmeo SARL, Geneva, Switzerland). Prior to *in vivo* use, evaluation of heating from components near the skin was performed using fiber-optic probes (AccuSens, Opsens Solutions, Montréal, QC, Canada). Human wrist MRI were acquired using the stitched, stretchable coil on the same scanner. The experimental procedures involving human subjects described in this paper were approved by the Institutional Review Board (protocol 19030219). The sagittal image was obtained using the same scan parameters mentioned above and the axial image was obtained using a T_1-weighted sequence with the following parameters: T_E 120 ms, slice thickness 2.5 mm, grid 512 × 512. Consistent with the phantom scans, the built-in body coil was used to transmit, while the stitched coil was receive-only.

III. Results

A. Coil Testing: Bench Measurements

Q-factor calculations from both the loaded and unloaded measurements and resulting SNR calculations are summarized in Table I below.

B. Coil Testing: MRI Experiments

Fig. 5 shows the resulting MR images gathered from the single-slice FSE sequence. All images have been set to have the same contrast and brightness for a faithful comparison.

Notable artifacts are produced in Fig. 5 by capacitors C_1 located at the top of the coil and C_3 at the bottom of the coil. In order to deliberately visualize any extraneous fields that may be produced, the imaging slice was placed splitting the coil in half along the z-plane. While all of the coils do exhibit the same artifacts due to the capacitors, it does appear that the PCB coil has a greater signal value than the stitched coils. However, the calculated SNR are similar between the draped and PCB coils.

Select *in vivo* human wrist images are shown in Fig. 6. Clear distinction of the wrist anatomy and fine details, such as the porosity of the bone, can be seen. The subject was able to comfortably place their wrist at a 30° bend for the scan.

IV. Discussion

Due to the zigzag stitching method, the conductive thread is anchored only to the top of the fabric, while the only thread that would potentially come in contact with a subject is nonconductive bobbin thread. The thread and fabric are washable, providing a hygienic aspect to the utilization of these coils, assuming any lumped elements and accessory boards are designed to be detachable. The stitch pattern and thread have maintained their integrity across several stretched configurations.

In phantom experiments, coils were mounted on a half-cylindrical shell to maintain a consistent stretch and coil size for the stitched coils. This maintenance of size was crucial for matching and tuning, as well as maintaining such during the scans. To address variability in operating frequency due to coil stretching, strategies may be employed to dynamically match the coil, e.g., piezoelectric actuators [15] or PIN diode circuit switches [16]. The stitched coils, both draped and stretched, exhibited similar Q-factor values to the comparison PCB coil when loaded. There is a substantially higher unloaded Q-factor for the PCB coil when unloaded, which was expected given the lower resistivity of the copper trace compared to the conductive thread.

Given the close proximity to the phantom, unshielded capacitors may affect image quality. Because artifacts are seen where the capacitors are placed (the spacing between the artifact sources was consistent with coil diameter), it would be beneficial to shield these components. The stretched coil did exhibit more noise than the draped coil indicating that stretching to the maximum capacity could impact image quality. The stretched-coil radius is approximately 26% larger than the radius of the draped-coil. With a larger coil, there is an increase in the total noise volume, yielding a lower SNR. To verify that it was the coil size that impacted loaded SNR values in stitched and draped positions, comparison between the flux densities, B_1, using the Biot-Savart law was performed. The flux density should be proportional to the loaded SNR measurements. This correlation was confirmed, as the ratio of stretched to draped B_1 and SNR_{loaded} is 1.24 Additionally, the increase in coil size increases the inductance of the coil and the Q-factor, which is reflected in Table I.

The Q-factor and SNR calculations for the PCB coiled spaced 4.2 cm above the phantom are important in illustrating that the coil proximity of placement to the skin has an impact on image quality. Even with a higher Q-factor than the stitched, stretchable coils, the SNR (Table II) was lower for the spaced PCB coil when compared to both stretchable coil configurations. This supports the notion that coils designed to custom fit the anatomy of interest would yield better images over rigid counterparts because they allow closer placement to the skin.

An RF coil that is both stretchable and flexible may increase the utility of MRI for a broader range of applications beyond joint disease and injury. For example while mammography has been the conventional method for breast cancer detection since the 1960s, MRI offers superior sensitivity, especially for denser breasts, and is recommended annually for screening high-risk women [17], [18]. Accordingly, a fully stretchable coil design may offer improvements for breast MRI across the diversity of forms and tissue densities present in the population, with enhanced SNR from the close skin placement.

The stretchable coils presented herein may be utilized to fabricate an array of receive elements. Orthogonal geometric decoupling between elements may be exploited for low-channel count arrays, while several techniques may be employed for high channel count arrays, e.g., element overlap [19], resonant inductive decoupling [20], or self-decoupling through mutual impedance cancellation [21].

V. Conclusion

Our research shows that this conductive thread and athletic material is a viable combination for an entirely stretchable coil, producing comparable SNR values and high-resolution *in vivo* images. This omnidirectional stretchable coil not only provides a significant advantage in the variety of positioning available across anatomy, but also for patient comfort.

Acknowledgments

Research supported by the National Institute of Biomedical Imaging and Bioengineering of the National Institutes of Health (No. R03EB026231).

References

[1]. Kaukinen P et al., "Magnetic resonance imaging (MRI)-defined cartilage degeneration and joint pain are associated with poor physical function in knee osteoarthritis – the Oulu Knee Osteoarthritis study," Osteoarthr. Cartil, vol. 25, no. 11, pp. 1829–1840, 11 2017. [PubMed: 28698105]

[2]. Hetherington HP, Avdievich NI, Kuznetsov AM, and Pan JW, "RF shimming for spectroscopic localization in the human brain at 7 T," Magn. Reson. Med, 2010

[3]. Corea JR, Lechene PB, Lustig M, and Arias AC, "Materials and methods for higher performance screen-printed flexible MRI receive coils," Magn. Reson. Med, vol. 78, no. 2, pp. 775–783, 8 2017 [PubMed: 27612330]

[4]. Nordmeyer-Massner JA et al., "MR imaging of healthy knees in varying degrees of flexion using a stretchable coil array provides comparable image quality compared to a standard knee coil array," Eur. J. Radiol, vol. 85, no. 3, pp. 518–523, 3 2016. [PubMed: 26860662]

[5]. Port A et al., "Towards wearable MR detection: A stretchable wrist array with on-body digitization," in Proc. Intl. Soc. Mag. Reson. Med 26, 2018.

[6]. Zhang B, Sodickson DK, and Cloos MA, "A high-impedance detector-array glove for magnetic resonance imaging of the hand," Nat. Biomed. Eng, vol. 2, no. 8, pp. 570–577, 8 2018. [PubMed: 30854251]

[7]. Cuthbertson JD et al., "The iPRES-W AIR Coil : A Flexible RF Coil for Simultaneous MR Image Acquisition, Wireless Communication, and Localized B 0 Shimming," pp. 3–4.

[8]. "Arthritis By the Numbers: Book of Trusted Facts & Figures," Sci. Am, vol. 310, no. 5, pp. 20–20, 4 2014.

[9]. Shapiro L, Staroswiecki E, and Gold G, "Magnetic Resonance Imaging of the Knee: Optimizing 3 Tesla Imaging," Semin. Roentgenol, vol. 45, no. 4, pp. 238–249, 10 2010. [PubMed: 20727453]

[10]. Keil B, "Construction of Receive Arrays," 21st ISMRM Weekend Educ. Course, 2013.

[11]. Doty FD, Connick TJ, Ni XZ, and Clingan MN, "Noise in high-power, high-frequency double-tuned probes," J. Magn. Reson, 1988.

[12]. Duan Q et al., "Characterization of a dielectric phantom for high-field magnetic resonance imaging applications," Med. Phys, 2014.

[13]. Hasgall P et al., "IT'IS Database for thermal and electromagnetic parameters of biological tissues, Version 4.0," IT'IS, 2018.

[14]. NEMA, "NEMA Standards Publication MS 6–2008 (R2014) Determination of Signal-to-Noise Ratio and Image Uniformity for Single-Channel Non-Volume Coils in Diagnostic MR Imaging," NEMA MR Stand. MS 6–2008, vol. C, 2008

[15]. Keith GA, Rodgers CT, Hess AT, Snyder CJ, Vaughan JT, and Robson MD, "Automated tuning of an eight-channel cardiac transceive array at 7 tesla using piezoelectric actuators," Magn. Reson. Med, vol. 73, no. 6, pp. 2390–2397, 6 2015. [PubMed: 24986525]

[16]. Ha S, Hamamura MJ, Nalcioglu O, and Muftuler LT, "A PIN diode controlled dual-tuned MRI RF coil and phased array for multi nuclear imaging," Phys. Med. Biol, vol. 55, no. 9, pp. 2589–2600, 2010. [PubMed: 20393229]

[17]. Siu AL, "Screening for Breast Cancer: U.S. Preventive Services Task Force Recommendation Statement," Ann. Intern. Med, vol. 164, no. 4, p. 279, 2 2016. [PubMed: 26757170]

[18]. Kuhl CK, Strobel K, Bieling H, Leutner C, Schild HH, and Schrading S, "Supplemental Breast MR Imaging Screening of Women with Average Risk of Breast Cancer," Radiology, 2017.

[19]. Roemer PB, Edelstein WA, Hayes CE, Souza SP, and Mueller OM, "The NMR phased array," Magn. Reson. Med, 1990.

[20]. Avdievich NI, Pan JW, and Hetherington HP, "Resonant inductive decoupling (RID) for transceiver arrays to compensate for both reactive and resistive components of the mutual impedance," NMR Biomed, 2013.

[21]. Yan X, Gore JC, and Grissom WA, "Self-decoupled radiofrequency coils for magnetic resonance imaging," Nat. Commun, vol. 9, no. 1, p. 3481, 12 2018. [PubMed: 30154408]

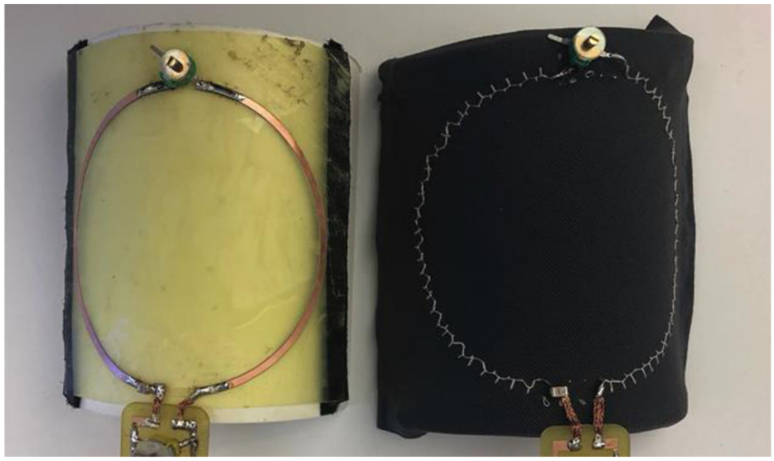

Figure 1.
Side-by-side comparison of PCB coil (left) and a draped, stitched stretchable coil (right).

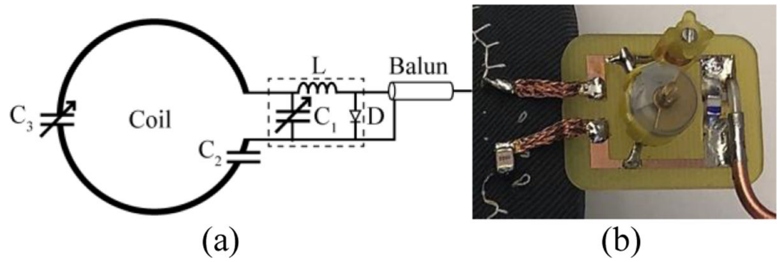

Figure 2.

(a) Schematic for the coil, match/tune board, and upstream connection to the balun. The dashed region identifies the trap comprised of L, C_1, and D. C_3 is utilized for tuning and C_2 for matching (b) Detailed view of the match/tune board with the incorporated current trap and capacitor, C_2, adjacent to the board.

Figure 3.

Scanning setup with the stretchable coil loaded/draped on phantom and connection to receive gateway.

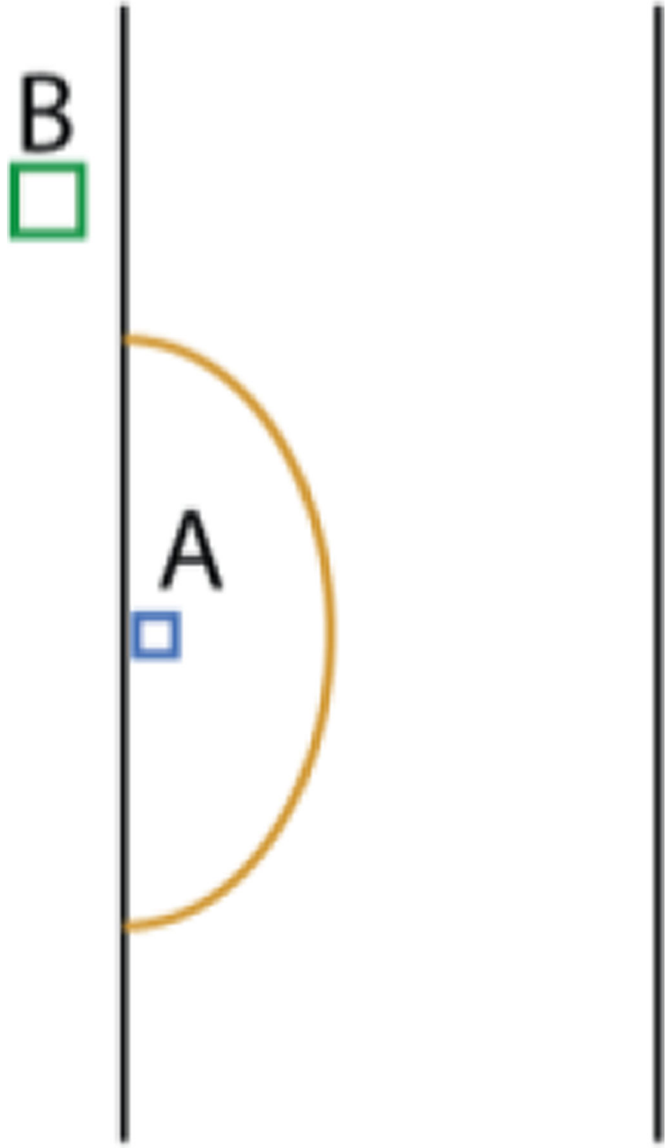

Figure 4.
Positions of signal (A, blue) and noise regions (B, green) for calculating mean signal and noise standard deviation values. The black lines denote the boundary of the phantom and the coil is depicted in orange.

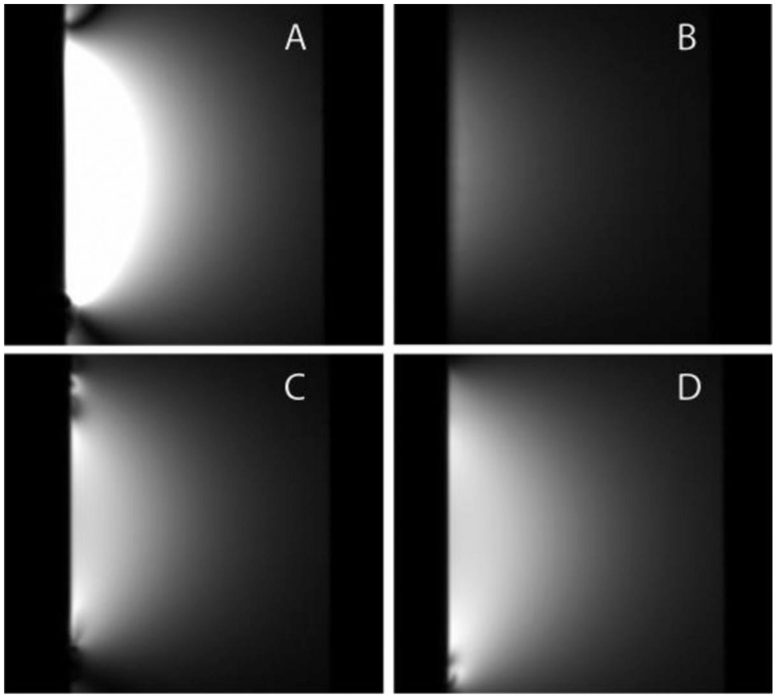

Figure 5.
FSE phantom images using (A) PCB coil, (B) PCB coil spaced 4.2 cm from phantom, (C) Stitched-draped coil, (D) Stitched-stretched coil.

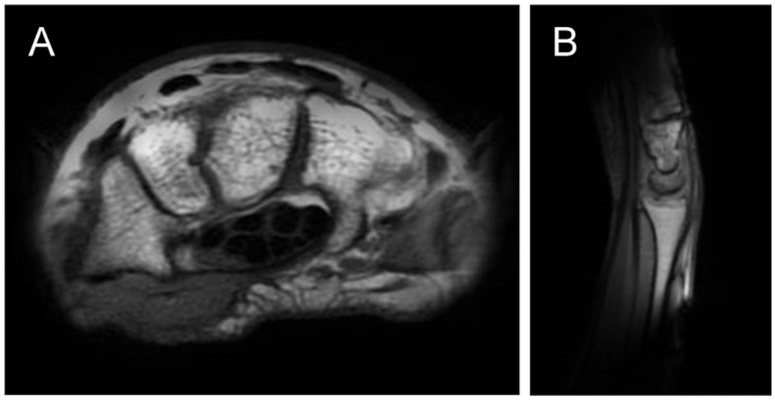

Figure 6.
Human wrist images using the stitched coil (wrist positioned at 30˚ bend): (A) Axial T_1-weighted image, (B) Sagittal FSE image.

TABLE I.

Q-Factor and SNR Calculations

Coil	Q-factor Loaded	Q-factor Unloaded	SNR
PCB	45.8	153	915
PCB (Spaced 4.2 cm)	116	153	665
Stitched (Draped)	35.4	53.0	835
Stitched (Stretched)	37.5	65.3	778